

Noise and aliases in off-axis and phase-shifting holography

M. Gross and M. Atlan

*Laboratoire Kastler-Brossel, Laboratoire de Physique de l'École Normale Supérieure,
Centre National de la Recherche Scientifique UMR 8552,
Université Pierre et Marie Curie, 24 rue Lhomond 75231 Paris cedex 05. France*

E. Absil

*Laboratoire d'Optique, École Supérieure de Physique et de Chimie Industrielles de la Ville de Paris,
Centre National de la Recherche Scientifique UPR A0005,
Université Pierre et Marie Curie, 10 rue Vauquelin 75231 Paris cedex 05. France*

(Dated: April 14, 2008)

We have compared the respective efficiencies of off-axis and phase-shifting holography in terms of noise and aliases removal. The comparison is made by analyzing holograms of an USAF target backlit with laser illumination, recorded with a charge-coupled device camera. We show that it is essential to remove the LO beam noise, especially at low illumination levels.

OCIS codes : 090.0090, 120.5060.

I. INTRODUCTION

In digital holography, holograms are recorded by a charge-coupled device (CCD) array detector, and the image reconstruction is performed by a computer [1], with the major advantage of avoiding photographic processing.

Off-axis holography [2] is the oldest and the simplest digital holography technique [3, 4, 5]. In off-axis holography, like in holography with photographic plates [6], the reference or local oscillator (LO) beam is angularly tilted with respect to the object observation axis. It is then possible to record, with a single hologram, the two quadratures of the object complex field. Nevertheless, the object field of view is reduced, since one must avoid the overlapping of the image with the conjugate image alias [7]. Off-axis holography has been applied recently to particle [8], polarization [9], phase contrast [10], synthetic aperture [11], low-coherence [12, 13] and microscopic [13, 14] imaging.

In phase-shifting interferometry [15] and digital holography [16], one records several images with different phases of the LO beam to compute the object field in quadrature in an on-axis (or inline) configuration. Recording a hologram inline requires a very accurate phase shift between consecutive images since the conjugate image alias overlaps with the true image. Aliases are suppressed by making image subtraction. Phase-shifting holography has been applied to 3D [17, 18], color [19, 20], polarization [18], synthetic aperture [21], low-coherence [22], surface shape [23] and microscopic [17, 24] imaging.

Recently, we have combined the off-axis configuration [3, 4, 5] with our digital holography phase-shifting technique [21, 26] to record off-axis phase-shifting digital holograms [25]. We must notice here that our phase shifting technique minimizes phase errors [27]. In the analysis of the data, we have used a spatial filtering technique [7] to remove the zero order and twin image aliases in order to improve the image quality. By combining all these

techniques, we have performed digital holography with ultimate sensitivity [27] i.e. with an equivalent noise that reaches the quantum limit of one photo electron of noise per reconstructed pixel during the whole measurement time.

In the present paper, we propose to reanalyze the holographic data used in our previous paper [25] in order to discuss the respective merits of the different techniques we have combined, i.e. off-axis recording of the hologram, spatial filtering, 4-phase phase-shifting and low phase error. The discussion will concern mainly aliases removal and sensitivity. We have chosen to consider the data of our previous paper [25] in order to simplify the discussion, since we have demonstrated in that paper that these data are sufficient to get optimal sensitivity.

II. EXPERIMENTAL SET-UP

The holographic setup is sketched in Fig.1. It consists of an interferometer in which the beams reaching the detector are angularly tilted (off-axis configuration) and frequency-shifted (dynamic phase shift). This setup has been described in [25]. The main laser L is provided by a Sanyo DL-7140-201 diode laser ($\lambda = 780$ nm, 50 mW for 95 mA of current). It is split into an illumination beam (frequency ω_L , complex field E_L), and in a reference local oscillator (LO) beam (ω_{LO} , E_{LO}). The object to be imaged is a back-illuminated USAF target. The optical frequency of the object field E is the same as the illumination field (ω_L). A set of optical attenuators A (gray neutral filters) allows to reduce the illumination level. The CCD camera (PCO Pixelfly digital camera: 12 bit, frame rate $\omega_{CCD} = 12.5$ Hz, acquisition time $T = 125$ ms, with 1280×1024 pixels of $6.7 \times 6.7 \mu\text{m}^2$) records the hologram of the object, i.e. the object (E) versus LO (E_{LO}) field interference pattern. By using two acousto-optic modulators (AOM1 and AOM2, Crystal Technology: $\omega_{AOM1,2} \simeq 80$ MHz), the optical frequency ω_{LO} of

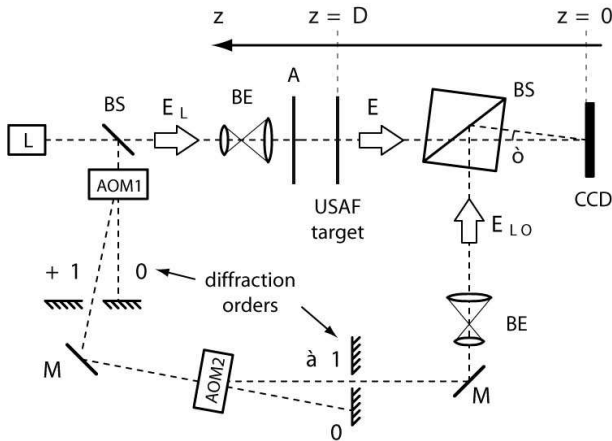


FIG. 1: Off-axis, dynamic phase-shifting digital holography setup. L: main laser; BS: Beam splitter; AOM1 and AOM2: acousto optic modulators (Bragg cells); BE: beam expander; M: mirror; A: light attenuator. USAF: transmission USAF 1951 resolution target. E_L , E_{LO} and E : illumination, local oscillator and object field. CCD: charge-coupled device array detector.

the LO beam, can be freely adjusted [27]. To make a 4-phase detection of the object field E , the LO frequency is detuned with respect to the object field optical frequency by :

$$\omega_L - \omega_{LO} = \omega_{AOM2} - \omega_{AOM1} \simeq \omega_{CCD}/4 \quad (1)$$

Moreover the LO beam is angularly tilted (angle $\theta \sim 1^\circ$) with respect to the camera-to-object observation axis, so that the object is seen off-axis with respect to the LO beam propagation axis. A sequence of 12 CCD images I_0 to I_{11} (measurement time 0.96s) is recorded, the phase being dynamically shifted by $\pi/2$ from one image to the next [27], as a consequence of appropriate frequency detuning (Eq.1). The interference pattern of the object with the LO field is carried by the frames I_m recorded by the camera at instants t_m .

$$t_m = 2\pi m / \omega_{CCD} \quad (2)$$

Let us introduce the complex representations \mathcal{E} and \mathcal{E}_{LO} of the signal and LO field envelopes.

$$E(t) = \mathcal{E}e^{j\omega t} + \mathcal{E}^*e^{-j\omega t} \quad (3)$$

$$E_{LO}(t) = \mathcal{E}_{LO}e^{j\omega t} + \mathcal{E}_{LO}^*e^{-j\omega t} \quad (4)$$

where $j^2 = -1$. The grabbed CCD signal is proportional to the field intensity.

$$I_m = |\mathcal{E} e^{j\omega t_m} + \mathcal{E}_{LO} e^{j\omega_{LO} t_m}|^2 \quad (5)$$

$$I_m = |\mathcal{E}|^2 + |\mathcal{E}_{LO}|^2 + \mathcal{E}\mathcal{E}_{LO}^* e^{j\omega_{CCD} t_m/4} + c.c. \quad (6)$$

where $c.c.$ is the complex conjugate of the $\mathcal{E}\mathcal{E}_{LO}^*$ term. In digital holography, the image is related to the $\mathcal{E}\mathcal{E}_{LO}^*$

term, while the zero order and twin images alias are related to the $|\mathcal{E}_{LO}|^2$ and $c.c.$ terms. The $|\mathcal{E}|^2$ is most often neglected. Moreover, with the choice of the LO frequency ω_{LO} , the $\mathcal{E}\mathcal{E}_{LO}^*$ phase factor becomes

$$e^{j\omega_{CCD} t_m/4} \simeq e^{jm\pi/2} = j^m \quad (7)$$

III. SINGLE PHASE, OFF-AXIS HOLOGRAPHIC IMAGES

In the collected data $\{I_0, \dots, I_{11}\}$, the LO beam is phase shifted by $\pi/2$ between consecutive images. To cancel the phase-shifting effect, we have selected images from the whole set of 12 recorded CCD frames for which the LO phase is the same : I_0, I_4 and I_8 . A single phase, off-axis hologram H in the CCD plane ($z = 0$) is formed as :

$$H(x, y, 0) = I_0(x, y) + I_4(x, y) + I_8(x, y) \quad (8)$$

We have reconstructed the images by using the standard convolution method [4, 28] that yields a calculation grid equal to the pixel size [29]. To calculate the convolution product, we have used the Fourier method, like in [26]. To avoid reconstruction aliases and to image an object larger than the CCD size we have enlarged our 1280×1024 measurement grid by padding the data into a 2048×2048 zero matrix [30] (zero padding), as seen on Fig.2a, where zero is black. Further calculations are done onto the 2048×2048 grid.

The reconstructed image is calculated by the following way. Eq.8 yields the real space hologram $H(x, y, 0)$ in the CCD plane. The hologram \tilde{H} in the CCD reciprocal plane (i.e. in the $z = 0$ k-space) is obtained by discrete Fourier transformation (FT):

$$\tilde{H}(k_x, k_y, 0) = \text{FT}[H(x, y, 0)] \quad (9)$$

The k-space hologram at any distance z from the CCD is then:

$$\tilde{H}(k_x, k_y, z) = \tilde{H}(k_x, k_y, 0) \exp(jz(k_x^2 + k_y^2)/k) \quad (10)$$

where $k = 2\pi/\lambda$ is the optical wave vector. The $\exp(jz(k_x^2 + k_y^2)/k)$ factor is the kernel function that describe k-space the propagation from 0 to z . The reconstructed image, which is the hologram in the object plane ($z = D$), is then obtained by reverse Fourier transformation:

$$H(x, y, D) = \text{FT}^{-1}[\tilde{H}(k_x, k_y, D)] \quad (11)$$

Fig.2a shows the digital hologram H of the USAF target recorded in the CCD plane. The hologram intensity $|H|^2$ is displayed in linear gray scale. Raw CCD frames (1280×1024 pixels) are padded within a 2048×2048 zero matrix displayed in black. Fig.2b shows the k-space hologram $\tilde{H}(k_x, k_y, 0)$, whose intensity $|\tilde{H}|^2$ is displayed in logarithmic scale.

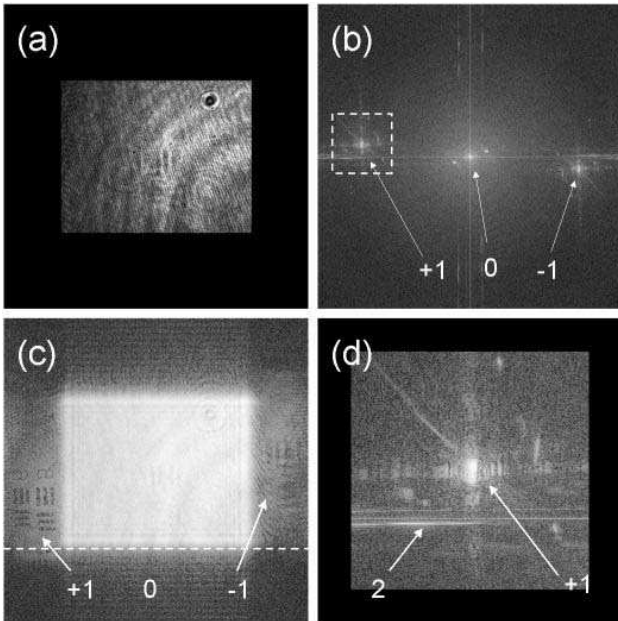


FIG. 2: Off-axis, single phase reconstruction of the target image. (a) Hologram $H(x, y, 0)$ that corresponds to the 1280×1024 CCD image padded in a 2048×2048 zero matrix (linear gray scale display). (b) k-space field (2048×2048 matrix, logarithmic gray scale for the intensity $|\tilde{H}|^2$). (c) image calculated on the 2048×2048 matrix with logarithmic gray scale display for the intensity $|H|^2$. (d) Enlargement of the k-space true image region (dashed rectangle in Fig.2b). The 400×400 pixels wide true image region is copied within a 512×512 zero matrix. The resulting 512×512 $|H|^2$ intensity image is displayed in logarithmic scale. (a,d) images correspond to a total signal of $\simeq 4.3 \times 10^8$ photo electrons for the sequence of 3 images.

The bright zone (arrow 0) in the center of Fig.2b corresponds to the FT of the LO beam ($|\mathcal{E}_{LO}|^2$ term) that is the zero order image. Because the LO beam is flat in the CCD plane, its Fourier counterpart yields a very narrow bright spot located in the center of the k-space, i.e. at $(k_x, k_y) \simeq (0, 0)$.

The relevant holographic signal, which corresponds to the $\mathcal{E}\mathcal{E}_{LO}^*$ interference term, is the bright zone of lower intensity, on the left hand side of the image (arrow +1). Because the LO beam is off-axis, the FT of the beat signal $\mathcal{E}\mathcal{E}_{LO}^*$ yields a signal shifted in k-space whose location can be precisely adjusted by tuning the angle between the LO and object beams (by tilting the beam splitter in front of the detector for example).

The twin image, which corresponds to the $\mathcal{E}^*\mathcal{E}_{LO}$ interference term, is symmetrical to the real image with respect to the k-space center (arrow -1 bright zone in the right hand side of the image). The angular tilt (represented by θ on Fig.1) between the object and the LO beam directions defines the separation distance between the true image, the twin image and the zero order image in k-space.

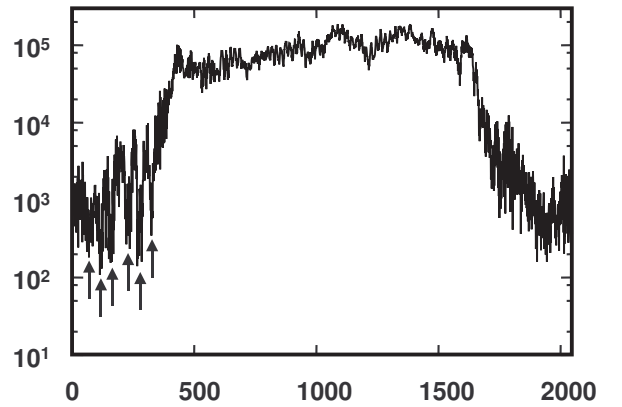


FIG. 3: Horizontal cut ($y \simeq 1196$) of the reconstructed field intensity $|\tilde{H}|^2$ of Fig.2c. Vertical axis is $|\tilde{H}|^2$ in Arbitrary Units (A.U.). Horizontal axis is pixel index $x = 0 \dots 2047$. Vertical display is logarithmic.

Fig.2c shows the reconstructed image of the USAF target whose intensity is displayed in logarithmic scale (i.e. $|\tilde{H}(k_x, k_y, z = D)|^2$). The true image (arrow +1) is on focus for a reconstruction distance $z = D = 215$ mm in Eq.10. The twin image (arrow -1) is blurred. It would be on focus for the reconstruction distance $z = -D$. The distance D and the off-axis angle θ are such that the true and twin images are partially masked by the zero order alias, which is much brighter than the USAF images (± 1 orders). Nevertheless because of the logarithmic display the USAF true and twin images are still visible in Fig.2c.

To perform quantitative study of the Fig.2 (c) image, we have represented an horizontal cut along the Fig.2 (c) dashed line. We have plotted on Fig.3 the reconstructed field intensity ($|\tilde{H}|^2$) trace at $y \simeq 1196$. To reduce the noise the curve is obtained by averaging over 11 pixels ($y = 1191$ to $y = 1201$). As seen on Fig.2c, the profile crosses 6 USAF black vertical bars, which are visible on the left hand side of the image. The profile crosses also the zero order image (white rectangle in the center of the image). On Fig.3, the zero order signal, which correspond to the central region of the curve ($x = 500$ to 1500), is much higher (about 10^5 A.U.) than the USAF signal (about 5×10^3 at maximum), which is visible on the curve left hand side ($x = 0$ to 400). The USAF bars (highlighted by arrows) are nevertheless visible on the curve.

To select the relevant first order image, and to fully suppress the zero order and twin image aliases, we have used, as proposed by Cuche et al. [7], a k-space filtering (or spatial filtering) method. We have selected, in the k-space 2048×2048 matrix $|\tilde{H}(k_x, k_y, z = 0)|^2$, a 400×400 region of interest centered on the true image bright zone (white dashed rectangle on Fig.2b). Note that this selection is made possible by the off-axis geometry that has translated the true image in the left hand side of the k-space domain. The selected area is then copied in the

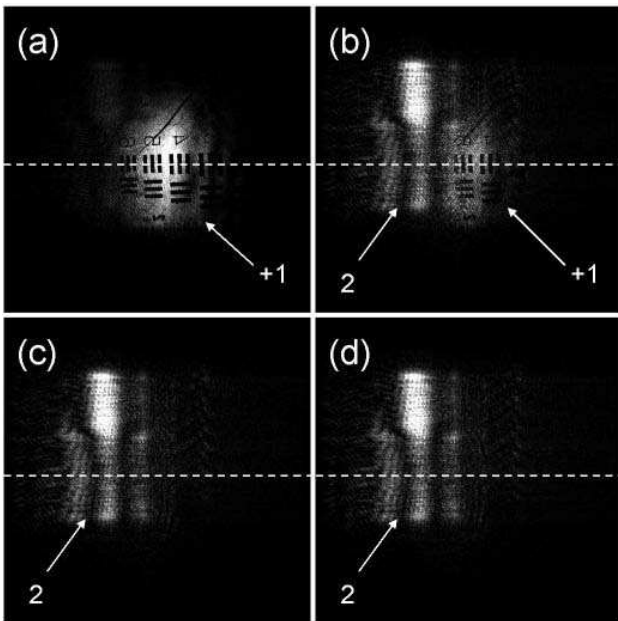


FIG. 4: Off-axis reconstructed image of a USAF target in transmission with low light illumination. Images are obtained with k-space filtering with $\simeq 4.3 \times 10^8$ (a), 8.7×10^6 (b), 8.7×10^4 (c) and 1.2×10^4 (d) photo electrons respectively for the sequence of 3 images. $|H|^2$ intensity displayed in linear gray scale.

center of a 512×512 zero matrix (zero padding) as shown on Fig.2d. The calculation of the $z = D$ k-space and real space holograms (Eq.10) are then done on this 512×512 calculation grid.

Fig.4a shows the object plane real space hologram $H(x, y, z)$ obtained by computing Eq.11, which yields the USAF target image. Note that the translation of the selected zone in the center of the k-space domain in Fig.2d moves the reconstructed image of the USAF target in the center of the image as seen in Fig.4a. The comparison of Fig.2c with Fig.4a illustrates the ability of the spatial filtering method [7] to improve the quality of the reconstructed image in single phase off-axis digital holography. Nevertheless, we will see that image quality will degrade when the illumination level becomes low.

The sensitivity limit of the single phase off-axis configuration was assessed by recording images of the USAF target at different levels of illumination. To get quantitative results, we have determined the absolute number of photo electrons that corresponds to the signal beam impinging onto the array detector. The calibration procedure is described in detail in reference [25]. Fig.4 shows the reconstructed images obtained for various attenuation levels. Although the Fig.4 b, c, d images are reconstructed with the same holograms as in reference [25], the calibration factor is slightly different. In reference [25], 12 holograms are used ($I_0 \dots I_{11}$) but the holographic data are truncated within a 1024×1024 calculation ma-

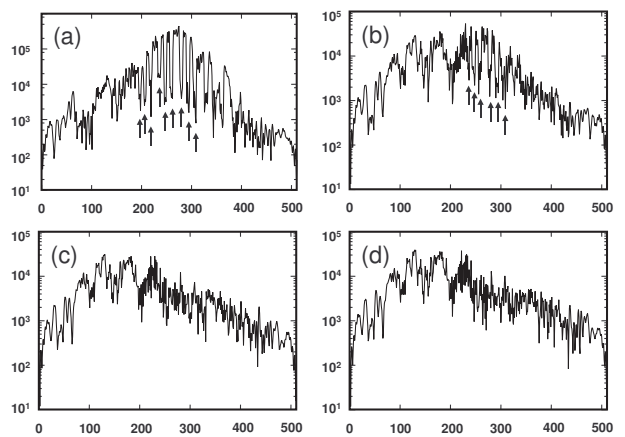


FIG. 5: Horizontal cuts ($y \simeq 264$) of the reconstructed field intensity $|\hat{H}|^2$ corresponding to the images Fig.4. (a) to (d) curves correspond to (a) to (d) images. Vertical axis is $|\hat{H}|^2$ in Arbitrary Units (A.U.). Horizontal axis is pixel index $x = 0 \dots 512$. Vertical display is logarithmic. The total signal is $\simeq 4.3 \times 10^8$ (a), 8.7×10^6 (b), 8.7×10^4 (c) and 1.2×10^4 (d) photo electrons respectively for the sequence of 3 images.

trix. Here, we make use of 3 CCD frames to form the holograms with the whole 1280×1024 pixel array (cf. Eq.8). The number of photo electrons is thus lowered by a factor $1280/(4 \times 1024) = 0.31$ in comparison with the results presented in reference [25].

On Fig.4a, with $\simeq 4.3 \times 10^8$ photo electrons for all the pixels of the set of 3 images (i.e. for $I_0 + I_4 + I_8$), one can see the USAF target with a good SNR (Signal to Noise Ratio). On Fig.4b, with 8.7×10^6 photo electrons, one can see the USAF target (arrow +1), but a parasitic signal is visible (arrow 2). When the illumination level goes down, the true image signal (arrow +1 in Fig.4a and b) decreases, while the parasitic signal (arrow 2 in Fig.4b, c and d) remains unchanged. The parasitic signal (arrow 2), which is visible on Fig.4b becomes then dominant on Fig.4c and d with 8.7×10^4 (c) and 1.2×10^4 (d) photo electrons, while the USAF target vanishes.

It is difficult to determine the exact nature of the parasitic signal. Nevertheless, since the parasites do not depend on the power of signal beam, they are related to the LO beam alone. We can thus simply conclude that off-axis holography with spatial filtering is not sufficient to remove all LO beam parasitic contributions of our experiment, and is thus unable to reach optimal detection sensitivity.

We have performed a more quantitative study of the off-axis images by performing cuts along the white dashed lines of Fig.4. The curves, which are obtained by averaging over 3 pixels ($y = 263$ to $y = 265$), are displayed on Fig.5. On curves (a) and (b) the signal is quite large ($\simeq 4.3 \times 10^8$ and 8.7×10^6 photo electrons in (a) and (b)) and the USAF target black bars are visible (see arrows on Fig.5). Nevertheless, because of the parasites, the 3

left hand side bars are not visible on curve (b). On curves (c) and (d) with 8.7×10^4 and 1.2×10^4 photo electrons respectively, the parasitic component is dominant, and the USAF bars are not visible.

The curves give the quantitative weights of the signal and parasitic components. Curves (b), (c) and (d) have roughly the same shape (except for the central region where the USAF bars are visible). This means that, when the signal is less than 8.7×10^6 photo electrons (curve (b)), most of the energy lies within parasitic contributions.

IV. PHASE-SHIFTING HOLOGRAPHIC IMAGES

As mentioned above, holographic images made from phase-shifting measurements are reconstructed by using the whole set of 12 recorded CCD frames. Since the LO beam is phase shifted by $\pi/2$ between consecutive images (see Eq.1), the object complex hologram H' is obtained by summing the CCD images with the appropriate phase shift $\Delta\varphi = -m\pi/2$, where $m = 0 \dots 11$ is the image index:

$$H'(x, y) = \sum_{m=0}^{11} (-j)^m I_m(x, y) \quad (12)$$

$$\begin{aligned} H' &= \sum_{m=0}^{11} (-j)^m \left(|\mathcal{E}|^2 + |\mathcal{E}_{LO}|^2 \right) \\ &+ \sum_{m=0}^{11} (-j)^m e^{+\omega_{CCD}t_m/4} \mathcal{E} \mathcal{E}_{LO}^* \\ &+ \sum_{m=0}^{11} (-j)^m e^{-\omega_{CCD}t_m/4} \mathcal{E}^* \mathcal{E}_{LO} \end{aligned} \quad (13)$$

By this choice of demodulation equation (Eq.12), the zero order image $|\mathcal{E}_{LO}|^2$ and the twin image $\mathcal{E}^* \mathcal{E}_{LO}$ terms are both zero, since $\sum_{m=0}^{11} (-j)^m = 0$, and $\sum_{m=0}^{11} (-j)^m e^{-\omega_{CCD}t_m/4} \simeq 0$. Moreover, the true image $\mathcal{E} \mathcal{E}_{LO}^*$ term is maximized, since $(-j)^m e^{+\omega_{CCD}t_m/4} \simeq 1$. If the 4-phase condition is not respected $\omega_L - \omega_{LO} \neq \omega_{CCD}/4$, the twin image term may differ from zero. This does not greatly affect the final result, since the zero order term, which is potentially much larger, still cancels.

Like in single phase off-axis holography, phase-shifting holograms are reconstructed by the convolution method that involves two FTs. The 1280×1024 pixels wide H' matrix is zero padded within a square 2048×2048 calculation grid and the FTs are calculated on this grid.

From the same data collected to assess the sensitivity limit of the single phase off-axis configuration, we have computed phase-shifting holograms of the USAF target for different levels of illumination, and we have reconstructed the images $H'(x, y, z = D)$ of the target without any spatial filtering.

Fig.6 shows the reconstructed images whose intensity $(|H'(x, y, D)|^2)$ is displayed in linear scale for $\simeq 1.7 \times 10^9$

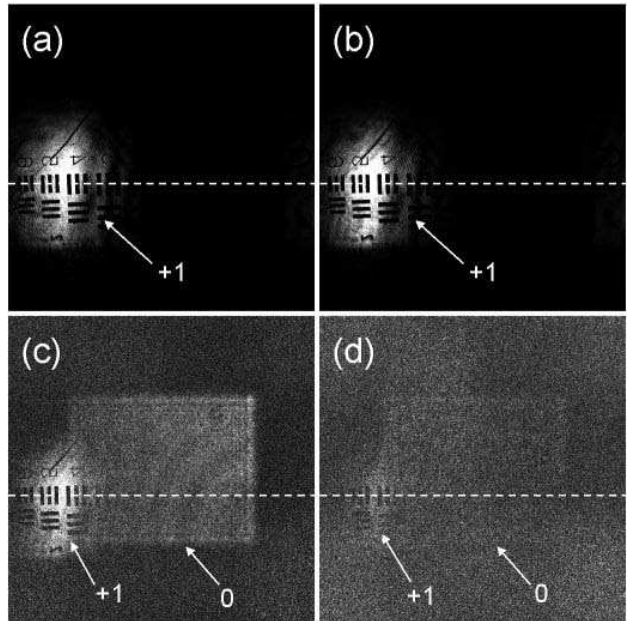


FIG. 6: 4-phase reconstructed image of a USAF target in transmission with low light illumination, without k-space filtering. Images are reconstructed with 1.7×10^9 (a), 3.5×10^7 (b), 3.5×10^5 (c) and 5×10^4 (d) photo electrons for all the pixels of the whole sequence of 12 images. $|H'|^2$ intensity displayed in linear gray scale.

(a), 3.5×10^7 (b), 3.5×10^5 (c) and 5×10^4 (d) photo electrons for all the pixels and all the 12 images of the sequence ($I_0 \dots I_{11}$). These figures correspond to the same attenuation level that are used in the single phase off-axis case, but the signal, in photo electron units, is four times larger, since the phase-shifting holographic images are obtained by using 12 CCD images instead of 3 previously. Note that the number of pixels used in the reconstruction calculation is slightly larger than in reference [25] (1280×1024 pixels instead of 1024×1024). As a consequence, for the same experimental data, the total number of signal photo electrons must be multiplied by a factor $\times 1.25$.

On Fig.6a and b, one see the USAF target with a good SNR. Since the object beam is angularly tilted by θ with respect to the LO beam, the USAF image is visible in the left hand side of the reconstructed image domain, but, contrarily to the Fig.2c off-axis image, the true image of the USAF target is visible without parasitic contribution. Thanks to heterodyne phase-shifting [26], the zero order and twin images are very low, and are thus not visible. On Fig.6c, with 3.5×10^5 photo electrons, the USAF target is visible, but the zero order image becomes visible too. On Fig.6d, with 5×10^4 photo electrons, the SNR is very low. One can only guess the USAF target image in the left hand side of the image.

The curves that are obtained by performing an horizontal cut ($y \simeq 1196$) and by averaging the signal intensity $|H|^2$ over 11 pixels ($y = 1191$ to $y = 1201$),

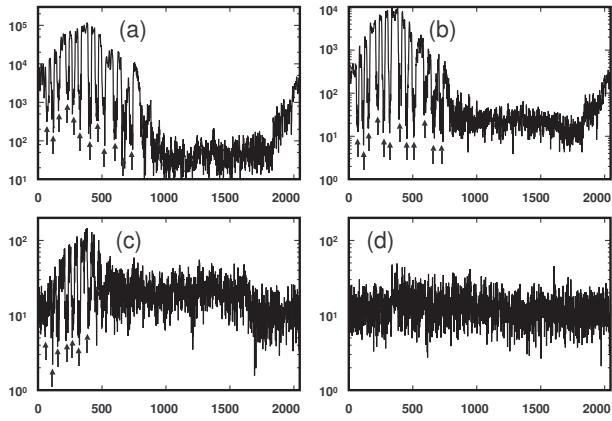


FIG. 7: Horizontal cuts ($y \simeq 1196$) of the reconstructed field intensity $|\hat{H}|^2$ corresponding to the 4 phase images of Fig.6. (a) to (d) curves correspond to (a) to (d) images. Vertical axis is $|\hat{H}|^2$ in Arbitrary Units (A.U.). Horizontal axis is pixel index $x = 0 \dots 2048$. Vertical display is logarithmic. The total signal is $\simeq 1.7 \times 10^9$ (a), 3.5×10^7 (b), 3.5×10^5 (c) and 5×10^4 (d) photo electrons for all the pixels of the whole sequence of 12 images.

are displayed on Fig.7. On curves (a), (b) and (c) with $\simeq 1.7 \times 10^9$, 3.5×10^7 and 3.5×10^5 photo electrons the USAF target black bars are clearly visible in the left hand side of the curves (see arrows on Fig.7). On curves (d) the signal is lower than the zero order image background and the bars are not visible.

Heterodyne phase-shifting is thus very efficient for getting good images at low illumination level. Phase-shifting holography is clearly better in our case than off-axis holography with or without spatial filtering. By making the difference of images in Eq.12 the $|\mathcal{E}_{LO}|^2$ term is cancelled, and most of the LO beam contribution to noise and parasitic signal is removed by phase-shifting holography. This is especially important at low illumination level, since, in that case, the LO beam, which brings noise and parasites, is of much larger power than the signal.

Since the phase-shifting holograms have been recorded in off-axis geometry, one can use the spatial filtering technique to improve further the quality of the reconstructed images, as done in reference [25]. We have selected in the k-space a 400×400 region centered on the true image, copied this region in the center of a 512×512 calculation grid (zero padding) and then calculated the USAF target images.

The reconstructed images are displayed on Fig.8 for the same levels of illumination that for Fig.6. Since the true image selected zone is translated in the center of the k-space domain, the USAF target is seen in the center of the reconstructed images. At high level of illumination, for $\simeq 1.7 \times 10^9$ (a) and 3.5×10^7 (b) photo electrons, the USAF images are seen with high SNR. The spatial filtering method does not seem to improve the image quality. On Fig.8 (c), with 3.5×10^5 (c) photo electrons, the

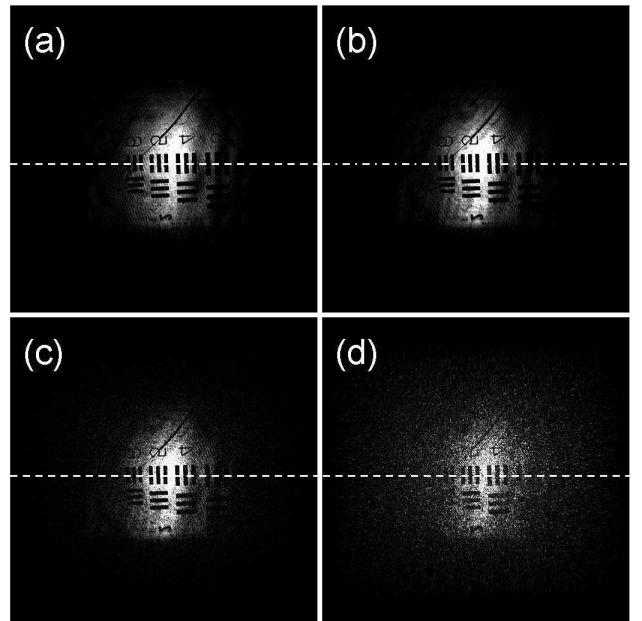


FIG. 8: 4-phase reconstructed image of a USAF target in transmission at low light illumination with k-space filtering. Images are reconstructed with $\simeq 1.7 \times 10^9$ (a), 3.5×10^7 (b), 3.5×10^5 (c) and 5×10^4 (d) photo electrons for all the pixels of the whole sequence of 12 images. $|H'|^2$ intensity displayed in linear gray scale.

USAF target is still seen with a good SNR. One can see that the image quality is better with spatial filtering (Fig.8 (c)) than without (Fig.6 (c)). Spatial filtering lowers the number of modes that bring noise, and cancels the zero order image that is seen on Fig.6 (c) (arrow 0, rectangular region). On Fig.8 (d), with 5×10^4 (c) photo electrons, the USAF target is still seen with $\text{SNR} \sim 1$. As explained in reference [25], the Fig.8 (d) image is obtained with about one photo electron per resolved pixel of the reconstructed image (or per k-space mode), for the whole sequence of 12 images.

The curves, which are obtained by averaging over 3 pixels ($y = 263$ to $y = 265$), are displayed on Fig.9. As seen, the USAF target black bars (see arrows) are easily visible on all curves. Image and cuts of Fig.8 and Fig.9, which have been obtained with the combination of techniques of reference [25] can be considered here as the optimal results to be reach.

V. DISCUSSION

Let us discuss on the respective merits of the techniques that are combined in reference [25] in order to get a shot-noise-limited holographic measurement.

As seen on the Fig.2 (c) reconstructed image, and on the Fig.3 cut, which are obtained with a large signal of 4.3×10^8 photo electrons, the LO beam zero order alias

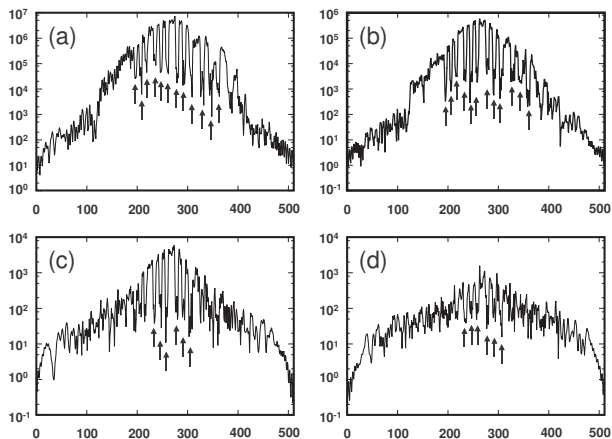


FIG. 9: Horizontal cuts ($y \simeq 264$) of the reconstructed field intensity $|\tilde{H}|^2$ corresponding to the images Fig.8. (a) to (d) curves correspond to (a) to (d) images. Vertical axis is $|\tilde{H}|^2$ in Arbitrary Units (A.U.). Horizontal axis is pixel index $x = 0 \dots 512$. Vertical display is logarithmic. The total signal is $\simeq 1.7 \times 10^9$ (a), 3.5×10^7 (b), 3.5×10^5 (c) and 5×10^4 (d) photo electrons for all the pixels of the whole sequence of 12 images.

is much brighter than the signal itself. This is confirmed by Fig.3. On the cut, the zero order alias (pixel 500 to 1600 plateau), is about 20 times larger than the signal itself (peaks and valleys marked by arrows, in the pixel 0 to 300 region). Moreover, the image and the zero order alias overlap. In single-phase regime, it is thus necessary to use a spatial filtering technique, as done on Fig.5 (a), in order to see the object without zero order alias overlapping. Such spatial filtering is nevertheless far to be sufficient to reach the shot noise limit with our experimental data, as shown by Fig.4 (c,d) and Fig.5 (c,d). By comparison, the 4-phase method without spatial filtering yields much better results. This is illustrated by comparing the Fig.4 and Fig.5 images and cuts, obtained with 1-phase holograms and spatial filtering, with the corresponding Fig.6 and Fig.7 images and cuts, obtained with 4-phase holograms, but without spatial filtering.

In the case of the 1-phase images and cuts presented on Fig.4 and Fig.5, the results are far from the shot-noise limit because of the parasites, visible on Fig.2 (d) (arrow 2). We have done many experiments with the setup sketched in Fig.1. With 1-phase, parasitic contributions are almost ever there, but their location depends on the beam splitter cube (BS) orientation. We guess that parasites are related to unwanted LO beam reflections on the BS, whose faces are not perfectly parallel.

To improve the quality of the 1-phase images, one can modify the BS orientation, such the k-space image of the object is moved in a "quiet zone" of the k-space, i.e. a zone without parasitic alias, like the upper right corner of the Fig.2 (b) k-space image. But this is not sufficient to reach the shot noise limit. To illustrate this point, we

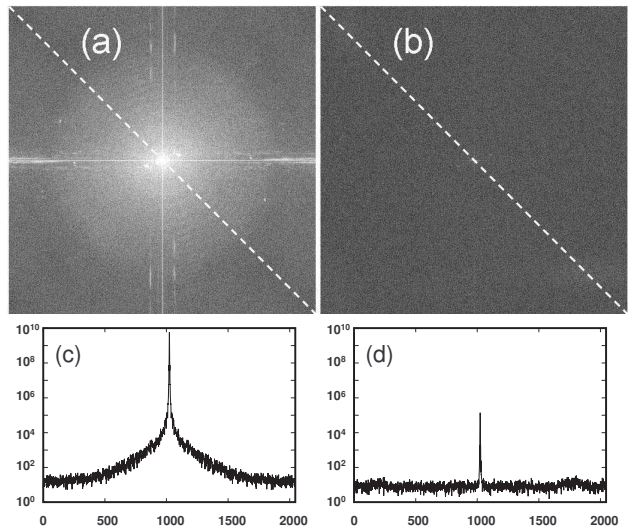


FIG. 10: (a,b) k-space field intensity $|\tilde{H}|^2$ and $|\tilde{H}'|^2$ reconstructed from 1-phase (a) and a 4-phase holograms obtained without signal (i.e. without illumination of the USAF char). (c,d) cut along the white dashed diagonal lines for 1-phase (c) and 4-phase (d) holograms. Vertical axis is k-space intensity $|\tilde{H}|^2$ and $|\tilde{H}'|^2$ along cut. Vertical axis is pixel index. Intensity is averaged over 11 pixels i.e. in the interval $(i, i - 5) \dots (i, +5)$ where $i = 0 \dots 2047$ is the pixel index.

have extracted, in the reference [25] experimental data, a sequence of 12 images without signal beam (i.e. with the LO beam alone). With these data, we have computed 1-phase and 4-phase holograms (Eq.8 and Eq.12, respectively). The k-space intensity images, $|\tilde{H}(k_x, k_y)|^2$ and $|\tilde{H}'(k_x, k_y)|^2$, are displayed on Fig.10 (a) and (b), with the same logarithmic gray scale.

With 1-phase (a), the LO beam image is much brighter, and extend over a much larger area, than in the 4-phase case (b). To make a quantitative analysis of these images, we have plotted profiles along the Fig.10 (a) and (b) white diagonal dashed lines. Note that we have made diagonal cuts in order to explore "quiet zones" of the k-space. The intensity signal ($|\tilde{H}|^2$ or $|\tilde{H}'|^2$) along the cut is represented on Fig.10 (c) and (d). For $k_x = k_y = 0$, we get a peak on the (c) and (d) cuts, which corresponds to the flat field component of the LO field. In the 1-phase case, the peak is about $\simeq 4 \times 10^4$ larger than in the 4-phase case. The 1-phase peak is also much broader, so that in most of the k-space domain, the 1-phase LO parasitic signal (c) is several orders of magnitude larger than its 4-phase counterpart (d). It is thus much larger than the shot noise limit, which is equal to the 4-phase noise floor (within a few per cent, as verified experimentally). The shot noise limit is thus not reached with 1-phase detection. This means that the LO beam signal cannot be fully filtered-off by spatial filtering. We guess that, in real life experiments, it is extremely difficult to have a perfect flat field LO beam. Thus, complete spatial filtering the

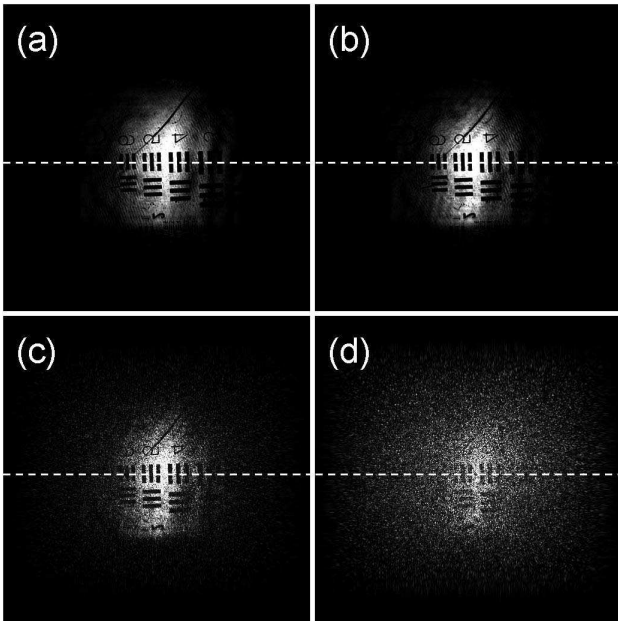


FIG. 11: 1-phase reconstructed images of a USAF target in transmission with subtraction of the average LO beam signal. Images are obtained with k-space filtering with $\simeq 4.3 \times 10^8$ (a), 8.7×10^6 (b), 8.7×10^4 (c) and 1.2×10^4 (d) photo electron respectively for the sequence of 3 images.

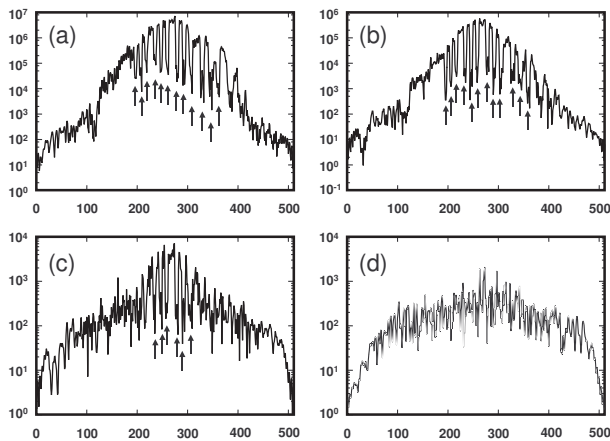


FIG. 12: Cuts of the 1-phase reconstructed images of the USAF target in transmission with subtraction of the LO beam signal. Images are obtained with k-space filtering with $\simeq 4.3 \times 10^8$ (a), 8.7×10^6 (b), 8.7×10^4 (c) and 1.2×10^4 (d) photo electron respectively for the sequence of 3 images.

LO beam cannot be achieved.

Performing a double filtering, in space and in time, is an efficient way to filter off the LO beam noise contributions. Quite good signal-to-noise levels can be obtained by the time domain filtering process which consist in subtracting the LO beam signal from the 1-phase hologram in order to cancel the $|\mathcal{E}_{LO}|^2$ term. To illustrate this

statement, we have calculated, from the sequence of 12 images, an approximation I_{LO} of the image that should be obtained with the LO beam alone. Since the phase of the hologram interference pattern is shifted by $\pi/2$ from one CCD image to the next, the CCD signal I_{LO} is:

$$I_{LO}(x, y) = \frac{1}{12} \sum_{m=0}^{11} I_m(x, y) \quad (14)$$

It is then possible to remove the LO beam signal on each CCD image. The corrected 1-phase hologram H'' is then :

$$H''(x, y, 0) = I_0(x, y) + I_4(x, y) + I_8(x, y) - 3I_{LO}(x, y) \quad (15)$$

$$H'' = \left(\sum_{m=0,4,8} + \frac{3}{12} \sum_{m=0}^{11} \right) (|\mathcal{E}|^2 + |\mathcal{E}_{LO}|^2) + \sum_{m=0,4,8} e^{+\omega_{CCD}t_m/4} \mathcal{E} \mathcal{E}_{LO}^* + c.c. \quad (16)$$

As seen, the $|\mathcal{E}_{LO}|^2$ zero order term cancels in H'' . From H'' , we have reconstructed LO-corrected 1-phase images and cut, which are shown on Fig.11 and Fig.12. The attenuation level (and thus the total signal in photo electron units) is the same than for the 1-phase images and cuts of Fig.4 and Fig.5. Here, the images and cuts quality is much better than without LO correction in Fig.4 and Fig.5. It is very close to the one obtained in the 4-phase configuration in Fig.6 and Fig.7. With respect to the 4-phase case, images and cuts are slightly noisier here simply because the signal is smaller by a factor 4, since the images are reconstructed from 4 times less CCD frames.

Note that these LO-corrected 1-phase results show that the phase accuracy in 4-phase holography is not essential. The phase accuracy has an effect on the weight of the twin image alias [27], but no significant effect on the weight of the zero order alias itself. To cancel the zero order alias, it is sufficient to build the hologram H' with difference of images such a way the $|\mathcal{E}|^2$ term is zero. This is ever realized whatever the image-to-image phase shift is, since $\sum_{i=0}^{11} (-j)^m = 0$ (see Eq.13).

VI. CONCLUSION

By comparing the reconstructed images obtained with holographic data measured in off-axis and phase-shifting configuration, we have shown that it is essential, for getting images with high SNR at low illumination levels to fully filter-off the LO beam. In off-axis holography, the LO beam yields the zero order image. It can be filtered off by numerical removal of its contribution in k-space domain (spatial filtering). This configuration also allows

the removal of the complex conjugate image. Nevertheless, this technique is not efficient enough to reach optimal sensitivity. This is particularly true when the camera exhibits image acquisition defaults. These defaults can be visualized during data analysis (see discussion about parasitic signal (arrow 2) visible on Fig.2(d)). In phase-shifting holography, the LO beam is filtered-off by making images differences. The LO beam component, which is the same on all the images, vanishes with images differences. Although more efficient, phase-shifting is not sufficient to fully cancel the LO beam contribution and its noise. Single filtering (in space or time) is thus not enough, and double filtering (in space and time) is needed if optimal sensitivity is required. The key point

of the time filtering process is to cancel the $|\mathcal{E}_{LO}|^2$ term in the equation yielding the hologram. We have to note that double filtering makes the measurement less prone to camera technical noise and parasites. The comparison of the images represented throughout this article, which are calculated from the same original data, is illustrative. Note that the quality of the phase shift in multiple-phase, off-axis holography is not essential, since quite as good results can be obtained with a single phase hologram by subtracting roughly the LO beam contribution.

The authors acknowledge support from the French National Research Agency (ANR) and the Centre de compétence NanoSciences Île de France (C'nano IdF).

-
- [1] J. W. Goodmann and R. W. Lawrence. Digital image formation from electronically detected holograms. *Appl. Phys. Lett.*, 11:77, 1967.
- [2] E.N. Leith, J. Upatnieks, and K.A. Haines. Microscopy by wavefront reconstruction. *J. Opt. Soc. Am.*, 55:981–986, 1965.
- [3] U. Schnars and W. Jüptner. Direct recording of holograms by a CCD target and numerical reconstruction. *Appl. Opt.*, 33(2):179–181, January 1994.
- [4] U. Schnars. Direct phase determination in hologram interferometry with use of digitally recorded holograms. *JOSA A.*, 11:977, July 1994.
- [5] T. M. Kreis, W. P. O. Juptner, and J. Geldmacher. Principles of digital holographic interferometry. *SPIE*, 3478:45, July 1988.
- [6] D. Gabor. Microscopy by reconstructed wave-fronts. *Proc. Royal Soc. London A*, 197:454–487, 1949.
- [7] E. CuChe, P. Marquet, and C. Depeursinge. spatial filtering for zero-order and twin-image elimination in digital off-axis holography. *Appl. Opt.*, 39(23):4070–4075, August 2000.
- [8] Y. Pu and H. Meng. Intrinsic speckle noise in off-axis particle holography. *JOSA A*, 21:1221–1230, 2004.
- [9] T. Colomb, P. Dahlgren, D. Beghuin, E. CuChe, P. Marquet, and C. Depeursinge. Polarization imaging by use of digital holography. *Appl. Opt.*, 41:27–37, 2002.
- [10] Etienne CuChe, Frédéric Belivacqua, and Christian Depeursinge. Digital holography for quantitative phase-contrast imaging. *Opt. Lett.*, 24(5):291–293, March 1999.
- [11] J. H. Massig. Digital off-axis holography with a synthetic aperture. *Opt. Lett.*, 27:2179–2181, 2005.
- [12] Z. Ansari, Y. Gu, M. Tziraki, R. Jones, P. M. W. French, D. D. Nolte, and M. R. Melloch. Elimination of beam walk-off in low-coherence off-axis photorefractive holography. *Optics Letters*, 26:334–336, 2001.
- [13] P. Massatsch, F. Charrire, E. CuChe, P. Marquet, and C. D. Depeursinge. Time-domain optical coherence tomography with digital holographic microscopy. *Appl. Opt.*, 44:1806, 2005.
- [14] P. Marquet, B. Rappaz, P. J. Magistretti, E. CuChe, Y. Emery, T. Colomb, and C. Depeursinge. Digital holographic microscopy: a noninvasive contrast imaging technique allowing quantitative visualization of living cells with subwavelength axial accuracy. *Opt. Lett.*, 30:468–470, 2005.
- [15] Katherine Creath. Phase-shifting speckle interferometry. *Applied Optics*, 24(18):3053, 1985.
- [16] I. Yamaguchi and T. Zhang. Phase-shifting digital holography. *Optics Letters*, 18(1):31, 1997.
- [17] T. Zhang and I. Yamaguchi. Three-dimensional microscopy with phase-shifting digital holography. *Opt. Lett.*, 23:1221–1223, 1998.
- [18] T. Nomura, B. Javidi, S. Murata, E. Nitandai, and T. Numata. Polarization imaging of a 3d object by use of on-axis phase-shifting digital holography. *Opt. Lett.*, 32:481–483, 2007.
- [19] Ichirou Yamaguchi, Tatsuki Matsumura, and Jun-Ichi Kato. Phase-shifting color digital holography. *Optics Letters*, 27(16):1108, July 2002.
- [20] J. Kato, I. Yamaguchi, and T. Matsumura. Multicolor digital holography with an achromatic phase shifter. *Opt. Lett.*, 27:1403–1405, 2002.
- [21] F. LeClerc, L. Collot, and M. Gross. Synthetic-aperture experiment in visible with on-axis digital heterodyne holography. *Optics Letters*, 26, October 2001.
- [22] S. Tamano, Y. Hayasaki, and N. Nishida. Phase-shifting digital holography with a low-coherence light source for reconstruction of a digital relief object hidden behind a light-scattering medium. *App. Opt.*, 45:953–959, 2006.
- [23] I. Yamaguchi, T. Ida, M. Yokota, and K. Yamashita. Surface shape measurement by phase-shifting digital holography with a wavelength shift. *App. Opt.*, 45:7610–7616, 2006.
- [24] P. Guo and A. J. Devaney. Multicolor digital holography with an achromatic phase shifter. *Opt. Lett.*, 29:857–859, 2004.
- [25] M. Gross and M. Atlan. Digital holography with ultimate sensitivity. *Opt. Lett.*, 32:909–911, 2007.
- [26] F. LeClerc, L. Collot, and M. Gross. Numerical heterodyne holography using 2d photo-detector arrays. *Optics Letters*, 25:716, Mai 2000.
- [27] M. Atlan, M. Gross, and E. Absil. Accurate phase-shifting digital interferometry. *Opt. Lett.*, submitted Feb 2007 ID: 79800.
- [28] T. Kreis. Digital holography for metrologic applications. in *Interferometry in Speckle Light*, P. Jacquot and J.-M. Fournier, eds., Springer Verlag, pages 205 – 212, 2000.
- [29] F. Zhang, I. Yamaguchi, and L. P. Yaroslavsky. Algo-

- rithm for reconstruction of digital holograms with adjustable magnification. *Opt. Lett.*, 29:1668–1670, 2004.
- [30] I. Yamaguchi, J. i. Kato, S. Ohta, and J. Mizuno. Image formation in phase-shifting digital holography and applications to microscopy. *Appl. Opt.*, 40(16):6177–6186, 2001.